

Deposition of TiO₂ Nanoparticles onto Silica Measured Using a Quartz Crystal Microbalance with Dissipation Monitoring

Julien Fatisson,[†] Rute F. Domingos,[‡] Kevin J. Wilkinson,[‡] and Nathalie Tufenkji*,[†]

[†]Department of Chemical Engineering, McGill University, Montreal, Quebec H3A 2B2, Canada, and

[‡]Department of Chemistry, University of Montreal, Montreal, Quebec H3C 3J7, Canada

Received December 11, 2008. Revised Manuscript Received March 22, 2009

Titanium dioxide (TiO₂) nanoparticles introduced into subsurface environments may lead to contamination of drinking water supplies and can act as colloidal carriers for sorbed contaminants. A model laboratory system was used to examine the influence of water chemistry on the physicochemical properties of TiO₂ nanoparticles and their deposition. Deposition rates of TiO₂ particles onto a silica surface were measured over a broad range of solution conditions (pH and ionic strength) using a quartz crystal microbalance with energy dissipation monitoring (QCM-D). Higher particle deposition rates were observed under favorable interaction conditions (i.e., in the presence of attractive electrostatic interactions) in comparison to unfavorable deposition conditions where electrostatic repulsion dominates particle–surface interactions. Nanoparticle sizes were characterized by fluorescence correlation spectroscopy (FCS), dynamic light scattering (DLS), and atomic force microscopy (AFM). These analyses confirmed the nanoscale of the system under study as well as the presence of TiO₂ aggregates in some cases. TiO₂ deposition behavior onto silica measured using QCM-D was generally found to be in qualitative agreement with the Derjaguin–Landau–Verwey–Overbeek (DLVO) theory of colloidal stability.

1. Introduction

The global market for nanotechnology was evaluated at \$9.4 billion in 2005 and is expected to increase to \$1 trillion by 2015.¹ Indeed, an increasing number of nanosized components are being incorporated into commercial products for performance enhancement. Engineered materials such as nanoparticles, nanorods, and nanotubes play a role in a wide range of domains including electronics, biomedical applications, cosmetics, pharmaceuticals, and energy. Although engineered nanomaterials hold great promise due to their unique physicochemical properties, little is known about their transport and fate in the natural environment or their potential cytotoxicity.²

The Organization for Economics Cooperation and Development (OECD) recently placed TiO₂ on its priority list of representative manufactured nanomaterials that require in-depth characterization (<http://www.olis.oecd.org>). TiO₂ is widely used in different commercial products, such as paints, sunscreens, and pigments. Although preliminary research reported by Wiesner and Bottero¹ demonstrates the ecotoxicity of TiO₂, the environmental fate and behavior of this nanomaterial has not been well characterized. A few studies have examined the transport and retention of TiO₂ nanoparticles in an effort to understand the contamination potential of this material in the natural subsurface environment.^{3–6}

Laboratory column and micromodel studies have been used to investigate the migration potential of TiO₂ nanoparticles in model granular porous media representative of the natural subsurface.^{3–6} This research showed that TiO₂ transport depended on solution pH⁴ and flow velocity in some cases,^{3,6} as observed for several other colloids or biocolloids in aqueous environments.^{7–9} Recently, in an extensive study of the aggregation behavior of TiO₂ nanoparticles,¹⁰ TiO₂ aggregation was shown to be most important at high solution ionic strengths and pHs close to its pH_{zpc}. Although some researchers have characterized the physicochemical properties and transport behavior of TiO₂ nanoparticles in granular porous media, our understanding of the deposition behavior of this material over a range of environmentally relevant conditions is incomplete.

In addition to the traditional laboratory column experiments, the quartz crystal microbalance has recently been shown to be an effective technique to monitor the attachment of molecules, particles, viruses, or cells onto clean or functionalized surfaces.^{11–18} Although the quartz crystal microbalance with dissipation monitoring (QCM-D) has been widely used to measure the

*Corresponding author. Telephone: (514) 398-2999. Fax: (514) 398-6678.
E-mail: nathalie.tufenkji@mcgill.ca.

(1) Wiesner, M. R.; Bottero, J.-Y. *Environmental Nanotechnology: Applications and Impacts of Nanomaterials*; The McGraw-Hill Companies: 2007; p 540.

(2) Nowack, B.; Bucheli, T. D. *Environ. Pollut.* **2007**, *150*(1), 5–22.

(3) Choy, C. C.; Wazne, M.; Meng, X. *Chemosphere* **2008**, *71*(9), 1794–1801.

(4) Dunphy Guzman, K. A.; Finnegan, M. P.; Banfield, J. F. *Environ. Sci. Technol.* **2006**, *40*(24), 7688–7693.

(5) Lecoanet, H. F.; Bottero, J.-Y.; Wiesner, M. R. *Environ. Sci. Technol.* **2004**, *38*(19), 5164–5169.

(6) Lecoanet, H. F.; Wiesner, M. R. *Environ. Sci. Technol.* **2004**, *38*(16), 4377–4382.

- (7) Li, X.; Johnson, W. P. *Environ. Sci. Technol.* **2005**, *39*, 1658–1665.
- (8) Abudalo, R. A.; Bogatsu, Y. G.; Ryan, J. N.; Harvey, R. W.; Metge, D. W.; Elimelech, M. *Environ. Sci. Technol.* **2005**, *39*, 6412–6419.
- (9) Ryan, J. N.; Elimelech, M. *Colloids Surf., A* **1996**, *107*, 1–56.
- (10) Domingos, R. F.; Tufenkji, N.; Wilkinson, K. J. *Environ. Sci. Technol.* **2009**, *43*(5), 1282–1286.
- (11) Chen, K. L.; Elimelech, M. *Langmuir* **2006**, *22*(26), 10994–11001.
- (12) Chen, K. L.; Elimelech, M. *Environ. Sci. Technol.* **2008**, *42*(20), 7607–7614.
- (13) Fatisson, J.; Merhi, Y.; Tabrizian, M. *Langmuir* **2008**, *24*(7), 3294–3299.
- (14) Lord, M. S.; Modin, C.; Foss, M.; Duch, M.; Simmons, A.; Pedersen, F. S.; Besenbacher, F.; Milthorpe, B. K. *Biomaterials* **2008**, *29*(17), 2581–2587.
- (15) Saleh, N.; Sirk, K.; Liu, Y.; Phenrat, T.; Dufour, B.; Matyjaszewski, K.; Tilton, R. D.; Lowry, G. V. *Environ. Eng. Sci.* **2007**, *24*(1), 45–57.
- (16) Stalgren, J. J. R.; Claesson, P. M.; Warnheim, T. *Adv. Colloid Interface Sci.* **2001**, *89*–90, 383–394.
- (17) Steinmetz, N. F.; Bock, E.; Richter, R. P.; Spatz, J. P.; Lomonosoff, G. P.; Evans, D. J. *Biomacromolecules* **2008**, *9*(2), 456–462.
- (18) Quevedo, I. R.; Tufenkji, N. *Environ. Sci. Technol.* 2009, in press.

adsorption kinetics of macromolecules such as proteins,^{19,20} few researchers have used this technique to monitor the deposition kinetics of nanoparticles.^{11,12,15,16,18} Chen and Elimelech^{11,12} used a QCM-D to examine the deposition kinetics of carbon-based (fullerene) nanoparticles in the presence of monovalent and divalent salts. In their work, the mass of nanoparticles deposited on a silica surface was related to the measured decrease in the resonance frequency of a QCM-D crystal. Quevedo and Tufenkji used a similar approach to quantify the deposition kinetics of a CdTe quantum dot over a broad range of water chemistries.¹⁸ Another approach to characterize particle or cell deposition/attachment using the QCM-D is the measurement of the energy dissipation factor, D .²¹

The purpose of this study is to examine the deposition rates of TiO₂ nanoparticles onto model sand (SiO₂) surfaces. The QCM-D was used to measure anatase TiO₂ deposition onto clean silica by following changes in the resonance frequency (f) and the energy dissipation factor (D) over a broad range of environmentally relevant solution chemistries, including variations in ionic strength, pH, and ion valence. The particle deposition behavior is related to variations in particle charge (evaluated using measurements of electrophoretic mobility) and particle size (determined by dynamic light scattering, DLS, and fluorescence correlation spectroscopy, FCS).

2. Materials and Methods

2.1. Preparation of Nanoparticle Suspensions. A stock suspension of TiO₂ (1 g/L) was prepared by suspending TiO₂ powder (reported diameter: 5 nm, NanoAmor) in deionized (DI) water. TiO₂ suspensions (10 mg/L) were prepared by diluting the stock suspension into a number of NaNO₃ (Sigma-Aldrich) solutions prepared at different salt concentrations ($I = 1\text{--}100$ mM) at pH 3.0 ± 0.1 . The suspension prepared at 10 mg/L (pH 3) was kept at 4°C overnight and then vigorously shaken using a vortex mixer set at high speed, and finally the pH was adjusted to 5 or 9 using 0.05 M NaOH (Fisher) 1 h prior to each experiment. The suspensions were gently mixed one additional time before conducting the experiments. All chemicals used to prepare solutions were of analytical grade.

2.2. Nanoparticle Sizing. Dynamic light scattering (Malvern ZetaSizer Nano) and fluorescence correlation spectroscopy (Leica TCS SP5 laser scanning microscope using ISS Vista FCS software, version 3.6) were used to measure the hydrodynamic diameters of the TiO₂. For FCS measurements, the TiO₂ particles were labeled using 10^{-8} M rhodamine 6G (Sigma-Aldrich), which corresponds to <0.1% surface coverage of the fluorophore. An optimized setting of 30–120 s was used for the acquisitions, with 15 repetitions. Excitation of the fluorophore was accomplished using an Ar ion laser at 514 nm, corresponding to the maximum excitation wavelength for this rhodamine derivative. All FCS measurements were performed at $22 \pm 1^\circ\text{C}$. Diffusion times were determined by calibrating the dimensions of the confocal volume using rhodamine 110 (Sigma-Aldrich), which has a known diffusion coefficient of 4.4×10^{-10} m²/s in water.²² Weight average diffusion coefficients were determined from the measured diffusion times across the calibrated confocal volume. DLS and FCS measurements were conducted using at least three independent samples.

2.3. Nanoparticle Imaging. Atomic force microscopy (AFM) and transmission electron microscopy (TEM) were also

employed to confirm the TiO₂ particle size distribution under selected conditions. For the AFM observations, TiO₂ suspensions were pipetted onto mica surfaces and left to sit for 4 h (Veeco Instruments Inc., NY) to allow particle deposition. The mica was air-dried and analyzed in tapping mode with standard silicon nitride cantilevers (Nanoworld). At least 20 images were taken of each particle covered mica sheet at a resolution of 256×256 pixels using a scan frequency of 1 Hz. AFM images were analyzed to determine individual particle sizes using image processing software (Image J).²³ Size distributions were determined from height measurements of a minimum of 140 particles from at least 20 independent AFM images of a single particle covered mica sheet. TEM was also used to obtain higher resolution images of the TiO₂ particles under selected conditions. In this case, samples were prepared by placing a drop of the TiO₂ suspension on a Formvar grid, which was left to air-dry overnight prior to analysis. Measurements were performed on a Philips CM200 microscope equipped with an AMT CCD camera and operating at 200 kV with a LaB₆ filament.

2.4. Electrokinetic Characterization of TiO₂ Particles. Laser Doppler velocimetry (ZetaSizer Nano ZS, Malvern) was used to characterize the electrophoretic mobility (EPM) of the nanoparticles in NaNO₃. Samples were briefly centrifuged to remove large aggregates (6200g, 1 min). EPM measurements were repeated using at least three different samples (prepared on different days) at $20.0 \pm 0.2^\circ\text{C}$. The strength of the applied electrical field (E) was 4.9 ± 0.1 V. Measured EPMs were converted to ζ -potential using the Smoluchowski equation.²⁴

2.5. Quartz Crystal Microbalance with Dissipation (QCM-D) Measurements. QCM-D measurements were performed with a Q-Sense E4 unit (Q-Sense AB, Göteborg, Sweden) by simultaneously monitoring the changes in frequency (Δf) and energy dissipation (ΔD) of a 5 MHz silica coated QCM-D crystal (QSX-303). The QCM-D crystal is excited to oscillate in the thickness-shear mode at its fundamental resonance frequency ($f_0 = 5$ MHz), at odd overtones ($n = 3, 5$, or 7) by applying a radio frequency voltage across the electrodes. Energy dissipation of the crystal is periodically recorded by measuring the exponentially dissipated sinusoidal voltage signal over the crystal caused by switching off the voltage applied to the piezoelectric oscillator. The Q-Sense software (QSoft) was then used to acquire the D factor via eq 1:

$$D = \frac{E_{\text{dissipated}}}{2\pi E_{\text{stored}}} \quad (1)$$

where $E_{\text{dissipated}}$ is the energy lost during one oscillation cycle and E_{stored} is the total energy stored in the oscillator. The D factor provides information on the deposition process as well as on some of the viscoelastic properties of the deposited layer. In the case of homogeneous, very thin, or quasi-rigid layers, the frequency shift of the oscillating crystal (Δf) can be related to the increase in mass per unit area, Δm_f , by the Sauerbrey²⁵ relationship:

$$-\Delta f = \frac{1}{nC} \Delta m_f \quad (2)$$

where the mass sensitivity constant, C , is equal to $17.7 \text{ ng}\cdot\text{cm}^{-2}\text{ Hz}^{-1}$ when $f = 5$ MHz. Prior to each experiment, the silica coated quartz crystals were cleaned in a UV-ozone chamber for 10 min. The crystals were then mounted in four separate QCM-D flow chambers, stabilized at $20.00 \pm 0.02^\circ\text{C}$, with only one side in contact with the working solution. A background NaNO₃ electrolyte at the pH and ionic strength of interest was injected at 0.40 mL/min until a stable baseline was reached. Subsequently, a

(19) Hook, F.; Voros, J.; Rodahl, M.; Kurrat, R.; Boni, P.; Ramsden, J. J.; Textor, M.; Spencer, N. D.; Tengvall, P.; Gold, J.; Kasemo, B. *Colloids Surf., B* **2002**, *24*(2), 155–170.

(20) Zhou, A.; Muthuswamy, J. *Sens. Actuators, B* **2004**, *B101*(1–2), 8–19.

(21) Poitras, C.; Tufenkji, N. *Biosens. Bioelectron.* **2009**, *24*, 2137–2142.

(22) Avaltroni, F.; Seijo, M.; Ulrich, S.; Stoll, S.; Wilkinson, K. J. *Biomacromolecules* **2007**, *8*(1), 106–112.

(23) Balnois, E.; Papastavrou, G.; Wilkinson, K. J. *IUPAC Ser. Anal. Phys. Chem. Environ. Syst.* **2007**, *10*, 405–467.

(24) Hunter, R. J. *Foundations of Colloid Science*, 2nd ed.; 2001; p 806.

(25) Sauerbrey, G. *Z. Phys.* **1959**, *155*, 206–22.

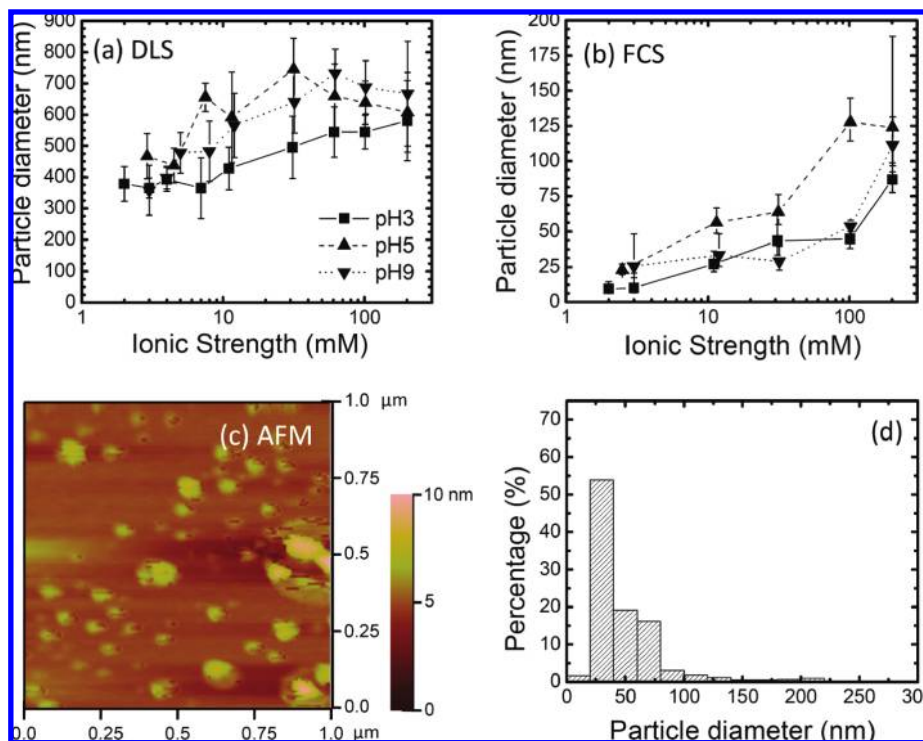


Figure 1. Measured TiO₂ particle size determined using several techniques: (a) DLS measurements of TiO₂ suspensions over a range of IS (NaNO₃) at pH 3 (■), pH 5 (▲), and pH 9 (▼); (b) FCS measurements over a range of IS (NaNO₃) at pH 3 (■), pH 5 (▲), and pH 9 (▼); (c) AFM height mode image of TiO₂ nanoparticles deposited onto mica from a 10 mg/L solution in 2 mM NaNO₃ at pH 3; (d) particle distribution obtained from analysis of 30 AFM height mode images for a 10 mg/L TiO₂ suspension deposited onto mica in 2 mM NaNO₃ at pH 3. Data represent the mean \pm 95% confidence interval.

suspension of TiO₂ particles in the same electrolyte was injected into the flow chambers (0.40 mL/min) for 20 min. Finally, the background electrolyte solution was injected at the same flow rate for 20 min. Frequency and dissipation shifts were continuously recorded during the entire experiment. QCM-D experiments were repeated using at least three different samples (prepared on different days). After each experiment, the crystals, chambers, and tubing were rinsed with 5 mL of 2% sodium dodecyl sulfate (SDS) (Sigma-Aldrich), 20 mL of DI, 5 mL of 2% Hellmanex (Fisher), and 30 mL of DI. Because the dissipation factor (D) is a ratio of energies (eq 1), it is dimensionless and is reported as 10⁻⁶ dissipation units (DU).

3. Results and Discussion

3.1. Characterization of TiO₂. *3.1.1. Sizing Analysis.* Particle size can play a critical role in the transport potential and environmental fate of colloids in aquatic systems.^{26–28} Moreover, it has been shown that the suspension preparation method can significantly influence the size and aggregation of TiO₂.²⁹ Hence, it is important to characterize the size of the particles used in this study in order to better understand the influence of solution chemistry on TiO₂ particle size and deposition behavior.

The nominal TiO₂ particle diameter reported by the manufacturer is 5 nm. Even after transformation to number average diameters, DLS measurements revealed particle sizes on the order of 350–750 nm (Figure 1a) depending on ionic strength and pH. Measured hydrodynamic diameters generally increased with increasing NaNO₃ concentration at each pH. The particles appeared smaller at pH 3 in comparison to the higher pHs. Because the scattering intensity of the particles is roughly proportional to

d^6 (Rayleigh approximation), DLS measurements are strongly influenced and highly sensitive to the presence of aggregates. Another investigation conducted under similar conditions has also reported the presence of TiO₂ aggregates using DLS.³⁰

Particle polydispersity has much less of an influence on hydrodynamic diameters determined by FCS³¹ as compared to diameters determined by DLS. Indeed, FCS determined weight averaged particle diameters were in the range of 7–189 nm (Figure 1b). Nonetheless, a similar trend of increasing particle size was observed with increasing salt concentration. No significant differences were observed between results acquired at pH 3 and pH 9; however, particle sizes at pH 5 were noticeably larger. Note that the FCS technique is somewhat limited for larger particles because the confocal volume can only accommodate a particle on the order of 200 nm in size.

As a third independent evaluation of particle diameter, AFM images were acquired for TiO₂ suspensions prepared for different solution chemistries (e.g., Figure 1c, 2 mM NaNO₃, pH 3). Height measurements of at least 140 particles were collected to produce particle size distributions (e.g., Figure 1d, 2 mM NaNO₃, pH 3). A large fraction of the TiO₂ particles had sizes below 50 nm with a smaller number of particles being observed in the larger size domains. Similar results were obtained for other solution conditions with average observed particle sizes of approximately 30 nm for all observations at pH 3 (10, 30, and 100 mM NaNO₃). Overall, particle sizes determined by AFM were in good agreement with FCS measurements, but they suggest that the suspensions could not simply be described by a single particle size. In another study, Choy et al.³ also observed the simultaneous

(26) Litton, G. M.; Olson, T. M. *Colloids Surf., A* **1996**, *107*, 273–83.

(27) Pelley, A. J.; Tufenkji, N. J. *Colloid Interface Sci.* **2008**, *321*(1), 74–83.

(28) Tufenkji, N.; Elimelech, M. *Environ. Sci. Technol.* **2004**, *38*(2), 529–536.

(29) Chen, X.; Mao Samuel, S. *Chem. Rev.* **2007**, *107*(7), 2891–959.

(30) Pettibone, J. M.; Cwiertny, D. M.; Scherer, M.; Grassian, V. H. *Langmuir* **2008**, *24*(13), 6659–6667.

(31) Starchev, K.; Buffle, J.; Perez, E. *J. Colloid Interface Sci.* **1999**, *213*(2), 479–487.

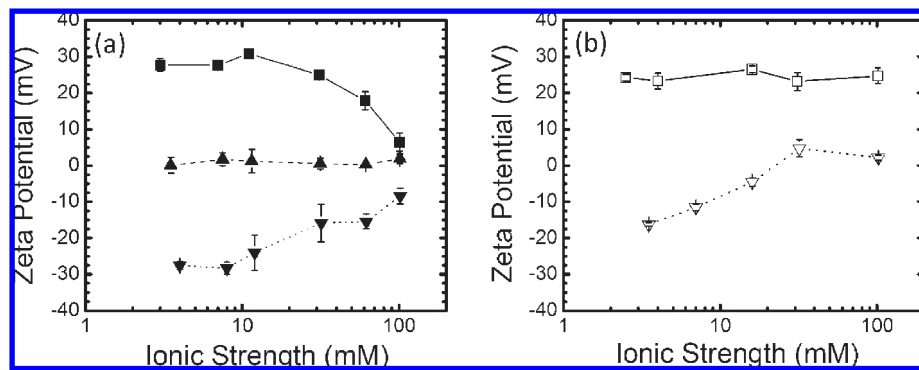


Figure 2. Calculated ζ -potentials from electrophoretic mobility measurements of TiO_2 particles over a range of I in (a) NaNO_3 at pH 3 (■), pH 5 (▲), and pH 9 (▼); (b) $\text{Ca}(\text{NO}_3)_2$ at pH 3 (□) and pH 9 (▽). Data represent the mean \pm 95% confidence interval.

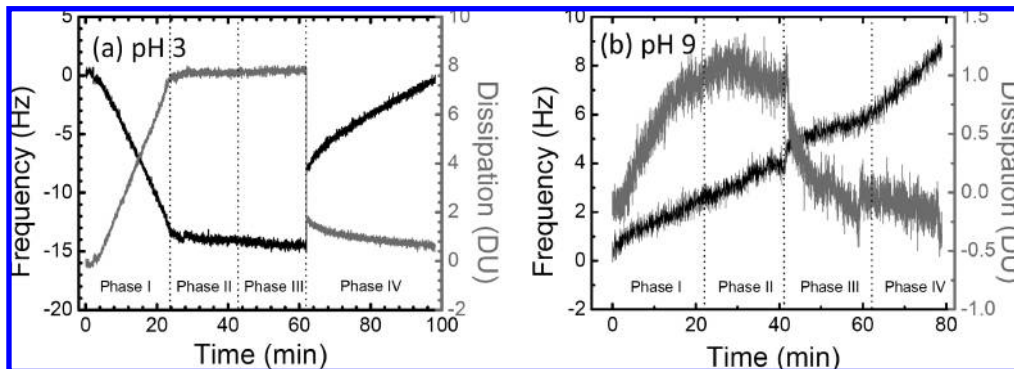


Figure 3. Representative QCM-D measurements (frequency and dissipation shifts, 3rd overtone) for deposition of TiO_2 onto SiO_2 coated QCM-D crystals. (a) Phase I: injection of TiO_2 particles suspended in 10 mM NaNO_3 at pH 3, phase II: injection of 10 mM NaNO_3 at pH 3, phase III: injection of 100 mM NaNO_3 at pH 3, and phase IV: injection of 10 mM NaOH (pH 12). (b) Phase I: injection of TiO_2 particles suspended in 100 mM NaNO_3 at pH 9, phase II: injection of 100 mM NaNO_3 at pH 9, phase III: injection of 10 mM NaNO_3 at pH 9, and phase IV: injection of 10 mM NaOH (pH 12). Baseline corrections have been made to take into account shifts in f and D resulting solely from changes in solution chemistry (i.e., in the absence of particles).

presence of TiO_2 aggregates and single particles in their study performed at pH 4.5, $I = 10$ mM.

TEM imaging carried out on selected samples confirmed the small nanometer sizes of the TiO_2 suspensions (Figure S1 in the Supporting Information). By combining all of the sizing techniques, it appears that the TiO_2 sample studied is mostly composed of very small particles (~ 30 nm) and a smaller number of aggregates between 100 and 500 nm in size and that more aggregates were present at pH 5. As mentioned above, the aggregates, even when present in small quantities, can create significant bias in the DLS measurements. FCS, AFM, and TEM analysis confirmed the presence of a large proportion of nanoparticles in the suspensions studied.

3.1.2. Electrophoretic Mobility (EPM) Measurements. Electrophoretic mobility measurements made for a large range of solution chemistries were converted to ζ -potentials (Figure 2). In the presence of the monovalent salt, at pH 3 and 5, the particles were positively charged while they were negative at pH 9, in accordance with previous studies conducted using anatase nanoparticles.^{32,33} Indeed, the measured EPM was near zero at pH 5, which is close to the pH_{Zpc} previously reported for nanosized anatase (5.8³⁴ and 5.1³⁵). In a related study, the EPM of the same TiO_2 product (from NanoAmor) was evaluated over a range of

pHs and the pH_{Zpc} was found to be in the range of 4.5–5.2.¹⁰ At the lowest and highest pH values, absolute ζ -potentials decreased with increasing ionic strength of the sodium salt, consistent with an increased charge screening. The ζ -potential and size data reported in Figures 1b and 2a are used later in the paper to interpret the results obtained by QCM-D within the context of Derjaguin–Landau–Verwey–Overbeek (DLVO) theory.

3.2. TiO_2 Deposition Kinetics on Clean Silica. 3.2.1.

Frequency and Dissipation Signals During TiO_2 Deposition onto Silica. Figure 3a shows representative QCM-D measurements following injection of a TiO_2 suspension at pH 3 in 10 mM NaNO_3 electrolyte. These conditions correspond to favorable conditions for deposition where attractive electrostatic interactions dominate the interaction between the particles and the silica surface. Following injection of the TiO_2 suspension into the QCM-D module, a decrease in frequency and an increase in dissipation are observed (phase I), resulting from nanoparticle deposition onto the silica surface. During phase II, a particle-free solution of NaNO_3 at the same I and pH is injected into the flow module, resulting in a stabilization in the frequency and dissipation shifts during this period (i.e., there is no change in attached mass at the crystal surface).

Because the frequency shift (Δf) is proportional to a change in mass (Δm) at the crystal surface (eq 2), the rate of change of Δf is equivalent to the rate of mass change on the crystal surface (i.e., the rate of particle deposition or release). Hence, the TiO_2 deposition rate can be determined by calculating the initial slope in the Δf plot (e.g., phase I in Figure 3a). The dissipation factor (D) also provides an indication of the mass attached to the crystal surface but also takes into account the “viscoelasticity” of the

(32) Gustafsson, J.; Mikkola, P.; Jokinen, M.; Rosenholm, J. B. *Colloids Surf., A* **2000**, *175*(3), 349–359.

(33) Ridley, M. K.; Hackley, V. A.; Machesky, M. L. *Langmuir* **2006**, *22*(26), 10972–10982.

(34) Pena, M.; Meng, X.; Korfiatis, G. P.; Jing, C. *Environ. Sci. Technol.* **2006**, *40*(4), 1257–1262.

(35) Kormann, C.; Bahnmann, D. W.; Hoffmann, M. R. *J. Phys. Chem.* **1988**, *92*(18), 5196–201.

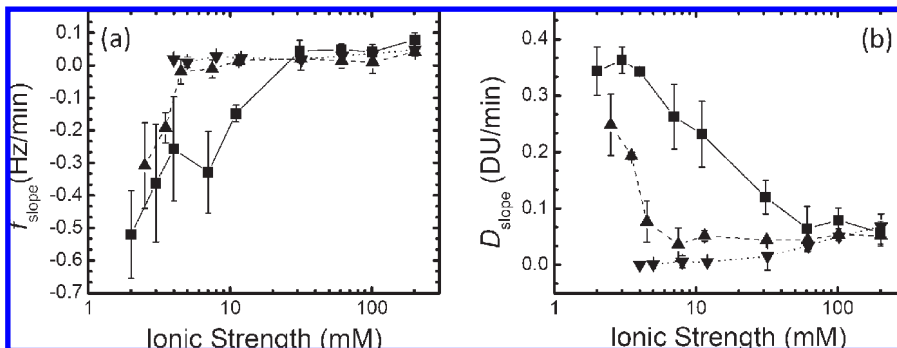


Figure 4. Average measured values of (a) f_{slope} and (b) D_{slope} determined from the 3rd overtone measurements during deposition of TiO_2 onto silica at different solution conditions: pH 3 (■ and solid line), pH 5 (▲ and dashed line), and pH 9 (▼ and dotted line). Data represent the mean $\pm 95\%$ confidence interval.

attached particle layer. The addition of a perfectly rigid mass to the crystal surface will yield zero additional D . However, the deposition of each particle onto the crystal surface can add a similar amount of energy loss which is reflected in D . Thus, the variation in ΔD with time can also be used as a means to evaluate the particle deposition rate (e.g., from the slope of the light gray curve in phase I of Figure 3a). To better understand how solution chemistry (pH and I) influences the TiO_2 deposition rate, the slopes of the frequency shift (f_{slope}) and the dissipation shift (D_{slope}) were calculated from the data obtained during the initial portion of phase I (e.g., Figure 4). Comparison of panels a and b in Figure 4 shows that the error bars obtained for at least three replicate measurements were generally wider in the case of the calculated f_{slope} than for the calculated D_{slope} (particularly at low I). This behavior has been reported previously³⁶ and indicates that, in some cases, the measurement of dissipation (D) can be a more reliable parameter than the measurement of resonance frequency. For example, Poitras and Tufenkji²¹ also demonstrated that the shift in dissipation was a more sensitive response signal than the frequency shift for detection of the bacterium *E. coli* O157:H7. Thus, for the sake of simplicity, D_{slope} has been chosen as the parameter of interest in the discussion that follows. However, it is important to note that the trends in f_{slope} are very similar to those observed for D_{slope} .

3.2.2. Effect of pH and Ionic Strength on TiO_2 Deposition.

Higher values of D_{slope} (and larger absolute values of f_{slope}) are indicative of higher TiO_2 deposition rates. Inspection of Figure 4b reveals higher values of D_{slope} under conditions where attractive electrostatic forces predominate; namely, when the surface is negatively charged and the particles are positively charged (at pH 3 and 5). At pH 3 and 5, D_{slope} decreases with increasing I , indicating lower TiO_2 deposition rates on the silica surface. As the ionic strength increases, the diffuse double layer is compressed, surface charges are screened, and consequently, the electrostatic attraction between the particle and surface is attenuated. This behavior is in qualitative agreement with DLVO theory (also see below) and several other studies examining colloidal deposition or aggregation under favorable conditions.^{37,38} Furthermore, at a given ionic strength, lower TiO_2 deposition rates were observed at pH 5 as compared to pH 3. In this case, the nanoparticles are less positive at pH 5 than at pH 3 (Figure 2a) and exhibit considerably more aggregation at pH 5 (Figure 1). Dunphy Guzman et al.⁴ also reported variations in TiO_2 deposition with changes in pH. These

trends will be explained in more detail within the context of DLVO theory later in the paper.

When repulsive electrostatic interactions dominate the particle–surface interaction (i.e., particles and silica surface are both negatively charged at pH 9), the TiO_2 deposition rate (i.e., D_{slope}) is near zero at low I . This observation can be explained by the fact that, at low I , the particle charge is not effectively screened and hence the electrostatic repulsion between the TiO_2 and the silica surface is strong. This behavior is consistent with a number of other studies examining particle or microbe deposition.^{7,9,39–41} As I increases, both particle and surface charges are more effectively screened as the thickness of the diffuse double layer decreases. Because repulsive forces are reduced, increased TiO_2 deposition results. This is demonstrated by the increase of D_{slope} with I at pH 9 (Figure 4b). It is interesting to note that the f_{slope} value at pH 9 was very low over the range of I and, in some cases, the values of f_{slope} were positive (Figure 4a). A positive value of f_{slope} is associated with a positive frequency shift. This behavior may be attributed to the formation of thick viscoelastic films on the crystal surface, or an apparently high viscosity at the liquid–crystal interface resulting from accumulation of weakly attached particles. Hence, the observed positive f_{slope} at pH 9 is consistent with the presence of electrostatic repulsive forces that can be expected when the silica surface and the TiO_2 particles are similarly charged.

At high I (i.e., above 100 mM), the rate of TiO_2 deposition represented by D_{slope} is similar (around 0.05 DU/min) for all examined pHs (Figure 4). As discussed, at high I ($I \geq 60$ mM), all charges are screened to the point that no significant differences can be observed between the particle deposition rates. Indeed, careful inspection of Figure 2a reveals that for all three pH values, ζ -potential values are approaching zero at the highest I .

For the system examined in this study, it is not straightforward to evaluate the mass of particles deposited on the silica surface from the raw QCM-D data. Difficulties arise in converting the measured f shifts to units of mass due to the inherent heterogeneity of the particle population (i.e., polydispersity) and the relatively high measured D shifts. The Sauerbrey relation (eq 2) is considered inappropriate for inhomogeneous films and likely underestimates the deposited mass in the system examined here. Nonetheless, if the Sauerbrey relationship was valid for this type of system, calculations show that the measured f shifts correspond to deposition rates of a few nanograms per minute (Table S1 in the Supporting Information).

(36) Fredriksson, C.; Khilman, S.; Kasemo, B.; Steel, D. M. *J. Mater. Sci.: Mater. Med.* **1998**, 9(12), 785–788.

(37) Elimelech, M.; Song, L. *Sep. Sci. Technol.* **1992**, 27(1), 2–12.

(38) Elimelech, M. *J. Colloid Interface Sci.* **1991**, 146(2), 337–352.

(39) Tufenkji, N.; Elimelech, M. *Langmuir* **2005**, 21(3), 841–852.

(40) Tufenkji, N. *Water Resour. Res.* **2006**, 42(12), W12S11.

(41) Johnson, W. P.; Li, X.; Assemi, S. *Adv. Water Resour.* **2007**, 30, 1432–1454.

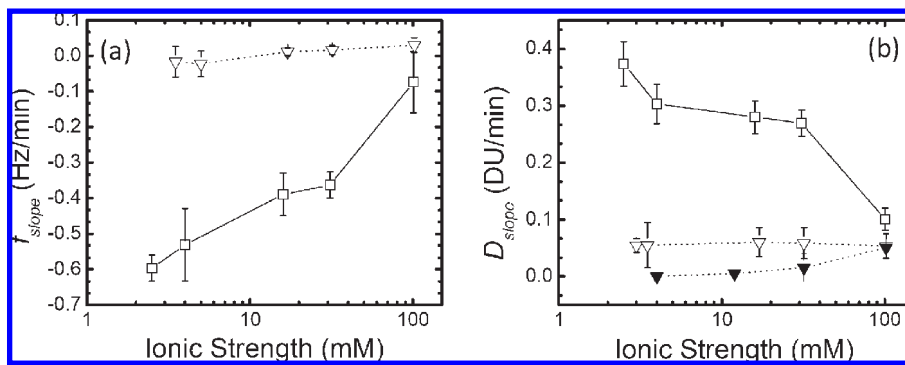


Figure 5. Average measured values of (a) f_{slope} and (b) D_{slope} (from 3rd overtone measurements) determined during deposition of TiO_2 suspended in a divalent salt ($\text{Ca}(\text{NO}_3)_2$) as a function of I at different pHs: pH 3 (□ and solid line) and pH 9 (▽ and dotted line). D_{slope} values from Figure 4 obtained at pH 9 (▼) have been added in (b) for direct comparison between monovalent and divalent salts. Data represent the mean \pm 95% confidence interval.

3.2.3. Effect of Ion Valence on TiO_2 Deposition. The influence of ion valence on TiO_2 ζ -potential and deposition kinetics was investigated by replacing the sodium salt (NaNO_3) with a calcium salt, $\text{Ca}(\text{NO}_3)_2$, for experiments run at pH 3 and 9 (Figures 2b and 5). The trends in the ζ -potentials in the presence of the divalent salt were similar to those observed in the presence of NaNO_3 . At pH 3, the particles were positively charged, while they were negative at the lower ionic strengths at pH 9 and became near-neutrally charged at the highest ionic strengths at pH 9 (Figure 2b). Experiments conducted at pH 3 with calcium nitrate showed a similar trend to those using sodium nitrate (Figure 5, open squares). At low ionic strength, the TiO_2 deposition rate is highest and in the same range as that observed with NaNO_3 . As the salt concentration increased, the value of D_{slope} , and correspondingly the particle deposition rate, decreased.

Experiments conducted at pH 9 in the presence of the calcium salt revealed no significant difference in the TiO_2 deposition rate over the range of I values examined (Figure 5, open inverted triangles). The particle deposition rate at this pH is close to the maximum obtained with NaNO_3 at pH 9, ~ 0.05 DU/min (Figure 5, solid triangles).

3.3. DLVO Interpretation of TiO_2 Deposition Kinetics. To better understand the mechanisms controlling the observed TiO_2 deposition behavior, DLVO theory was used to calculate colloidal interaction energies. DLVO theory considers the sum of London–van der Waals (VDW) and electrical double layer (EDL) interactions. The total interaction energy, namely, the sum of VDW and EDL interactions, was determined by treating the particle–silica system as a sphere–plate interaction. Constant-potential EDL interactions were calculated using the expression of Hogg et al.,⁴² where the ζ -potentials of the TiO_2 particles and the silica surface were used in place of the respective surface potentials. TiO_2 ζ -potentials were taken from Figure 2a, whereas silica ζ -potentials were taken from Bergna and Roberts⁴³ or extrapolated from the data of Walker et al.⁴⁴ The retarded VDW attractive interaction energy was calculated from the expression proposed by Gregory.⁴⁵ A value of 1×10^{-20} J was chosen for the Hamaker constant for the silica–water– TiO_2 system.⁴⁶ Nanoparticle sizes were taken from values obtained

from the FCS measurements (Figure 6a–c) or from the DLS measurements (Figure 6d–f) (Table S2 in the Supporting Information).

DLVO interaction energy profiles for the TiO_2 –silica system in the presence of a monovalent salt are presented in Figure 6. At pH 3 (Figure 6a,d), no energy barrier is present such that DLVO calculations predict completely favorable conditions for deposition of the positively charged particles onto the negatively charged silica surface. At this pH, the energy well forms at a larger particle–surface separation at 2 mM as compared to the higher ionic strengths. These calculations suggest that, for a TiO_2 particle approaching a silica surface, the attractive interaction will be felt at greater separation distances at an ionic strength of 2 mM as opposed to 100 mM. The calculated interaction energy profiles are consistent with the observed deposition rates for TiO_2 (i.e., 2 mM $>$ 10 mM $>$ 100 mM; Figure 4). Indeed, Elimelech and Song^{37,47} used theoretical calculations to show that attractive double layer interactions can extend to larger distances at lower I , thereby enhancing particle deposition.

At pH 5, the trends in the DLVO profiles are not in as good agreement with the deposition behavior when the particle size determined by FCS is used (Figures 4 and 6b); namely, the starting point of the energy well is not always located at greater separation distances at lower I . Also, the decay in the interaction energy profile appears slightly steeper at pH 5 (Figure S2 in the Supporting Information) than at pH 3, although greater particle deposition rates were noted at pH 3 in comparison to pH 5. It is important to note that the pH_{zpc} of TiO_2 is very near pH 5, and this is indeed the pH at which we observed important aggregation (Figure 2b). Indeed, aggregation is likely occurring over the time scale of the deposition experiments at this pH. The formation of aggregates can lead to decreased deposition due to decreased convective–diffusive transport to the silica surface as well as a decrease in the effective particle number concentration. Hence, the poorer agreement between DLVO calculations and QCM measurements at pH 5 may be attributed to the instability of the TiO_2 suspension at this pH. Nonetheless, the DLVO calculations determined using the particle size based on DLS (Figure 6e) are in good qualitative agreement with the particle deposition behavior.

At pH 9, the particles and the silica surface are both negatively charged, and hence, unfavorable conditions for deposition predominate (Figure 6c,f). The DLVO calculations presented in Figure 6c,f suggest that, at ionic strengths of 2 mM and 10 mM, the repulsive energy barrier will effectively prevent TiO_2 particles from depositing on the silica surface. Such a result is

(42) Hogg, R.; Healy, T. W.; Fuerstenau, D. W. *Trans. Faraday Soc.* **1966**, 62(6), 1638–1651.

(43) Bergna, H. E., Roberts, W. O., Eds. *Colloidal Silica: Fundamentals and Applications*; Surfactant Science Series 131: 2006; p 912.

(44) Walker, S. L.; Bhattacharjee, S.; Hoek, E. M. V.; Elimelech, M. *Langmuir* **2002**, 18(6), 2193–2198.

(45) Gregory, J. *J. Colloid Interface Sci.* **1981**, 83(1), 138–145.

(46) Feiler, A.; Jenkins, P.; Ralston, J. *J. Phys. Chem. Chem. Phys.* **2000**, 2(24), 5678–5683.

(47) Elimelech, M. *Sep. Sci. Technol.* **1994**, 4(4), 186–212.

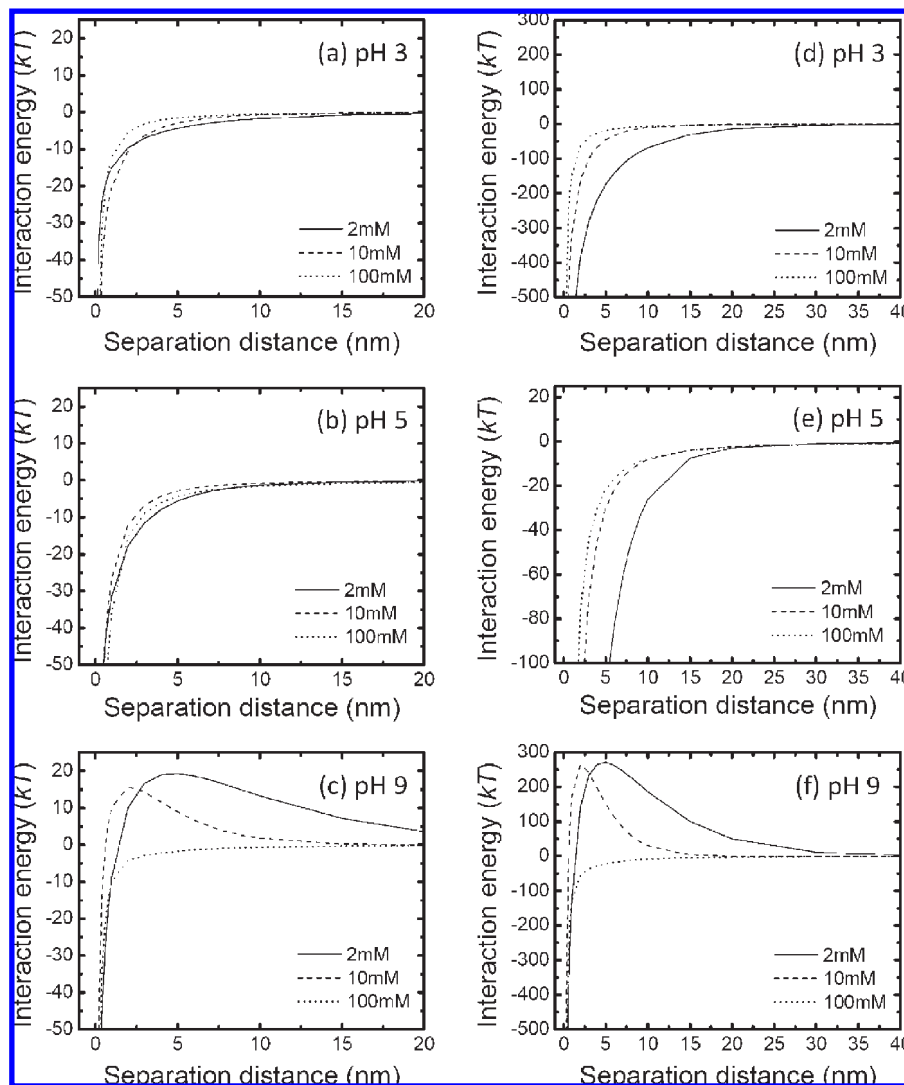


Figure 6. Calculated DLVO interaction energy profiles for a TiO_2 nanoparticle approaching a flat SiO_2 surface at (a) pH 3, (b) pH 5, and (c) pH 9 for different I values (NaNO_3): 2 mM (solid lines), 10 mM (dashed lines), and 100 mM (dotted lines). Nanoparticle sizes were taken from values obtained from the FCS measurements (Figure 1b) and are listed in Table S2 in the Supporting Information. Calculated DLVO interaction energy profiles for a TiO_2 particle approaching a flat SiO_2 surface at (d) pH 3, (e) pH 5, and (f) pH 9 for different I values (NaNO_3) using sizes obtained from the DLS measurements (Figure 1a) as listed in Table S2 in the Supporting Information.

consistent with QCM-D measurements that revealed little or no particle deposition at pH 9 at the low ionic strengths (Figure 4). On the other hand, when the salt concentration is increased to 100 mM, the repulsive energy barrier is eliminated (Figure 6c,f), and the conditions become more favorable for particle deposition, in agreement with measured values of D_{slope} . At the high ionic strengths, observations of similar deposition rates at each of the pH values (Figure 4) are explained by the fact that, at 100 mM, the DLVO interaction energy profiles are very similar for all three pH values (Figure S2c,f in the Supporting Information). In general, the DLVO calculations based on the two different sets of measured particle sizes (FCS versus DLS) are in good agreement, except at pH 5 where we note slight disagreement at the higher I . To our knowledge, this is the first attempt to characterize TiO_2 nanoparticle–silica interactions over a wide range of solution chemistries using DLVO theory. Although DLVO theory is useful for providing insight into the mechanisms controlling the particle deposition behavior, it is important to note the limitations of comparing the experimental QCM-D results to DLVO theory; for instance, the theory assumes the interaction of perfectly spherical,

uniformly sized particles with a flat and homogeneous collector surface.

3.4. Monitoring TiO_2 Detachment Using QCM-D. To better understand the risk of TiO_2 particle release from sand surfaces in aqueous environments, selected detachment experiments were also conducted using the QCM-D. For example, particle release from a surface can occur following specific changes in solution chemistry^{4,28,48} as a result of rainfall or due to surface water–groundwater exchange. In Figure 3a, TiO_2 particles were deposited in 10 mM NaNO_3 at pH 3 (phase I), followed by an injection of particle-free electrolyte at the same I and pH (phase II). During phase II of this favorable deposition experiment, there is no detectable change in the f or D shifts, indicative of no release of particles from the silica surface. In phase III, a particle-free solution of NaNO_3 at higher I (100 mM) and identical pH is injected into the flow module. Even though the solution chemistry has been changed in phase III, leading to changes in the particle and surface ξ -potential, there was no observable effect on the deposited particles. Because the particles

(48) Franchi, A.; O'Melia, C. R. *Environ. Sci. Technol.* **2003**, 37(6), 1122–1129.

deposited in phase I were deposited under completely favorable conditions, they are believed to be trapped in the primary energy well of the DLVO interaction energy profile (Figure 6a,d).

On the other hand, the strong interaction between the TiO_2 particles and the silica surface can be disrupted by a particle-free solution at higher pH and very low ionic strength (10 mM NaOH; pH 12) injected into the flow module (Figure 3a, phase IV). In this case, a rapid increase in frequency and a corresponding decrease in dissipation were observed during this phase of the experiment. At pH 12, both the particles and the silica surface are negatively charged such that the attractive interactions are replaced with strong repulsive electrostatic interactions.

Particles were generally released more readily when they were deposited under conditions deemed unfavorable (i.e., when repulsive electrostatic interactions predominate).⁴⁹ When TiO_2 particles were deposited at pH 9 and 100 mM NaNO_3 , detachment of the particles was observed during phase III when ionic strength was decreased to 10 mM (pH 9) (Figure 3b). Similar behavior has been observed when examining the deposition behavior of fullerene aggregates using QCM-D;¹¹ namely, the presence of repulsive interactions was sufficient to weaken attachment and led to particle detachment. This result is also in agreement with previous studies of particle deposition under unfavorable conditions^{49,50} which demonstrate that when the surface and particles are similarly charged, the deposition of particles is reversible and weaker than that observed when electrostatic interactions are attractive.

4. Conclusions

This study reports for the first time TiO_2 nanoparticle–silica interactions over a broad range of environmentally relevant solution pHs and ionic strengths. The slope in the dissipation shift (D_{slope}) from QCM-D measurements is shown to be a useful indicator of particle deposition behavior. Water chemistry was

shown to play a significant role on the TiO_2 deposition rate. Under favorable conditions for deposition (i.e., pH 3 and 5), the maximum deposition rate was observed at low ionic strength as a result of strong attractive electrostatic interactions between the nanoparticles and the surface. Increasing ionic strength led to a decrease in deposition rate when the particles and the surface were oppositely charged. The contrary was observed under unfavorable conditions, where the particles and the silica surface were similarly charged. Under these conditions, low deposition rates were measured at low ionic strength with particle deposition increasing at higher salt concentrations. In general, TiO_2 deposition kinetics, determined by measurements of the frequency and dissipation slopes, were in good qualitative agreement with classical DLVO theory at pH 3 and 9. This study also reports for the first time a comprehensive analysis of TiO_2 nanoparticle size using several complementary experimental techniques (DLS, AFM, FCS, and TEM) over a wide range of water chemistries. The results also highlight the limitations of DLS in characterizing polydisperse suspensions.

Acknowledgment. This work is supported by the Natural Sciences and Engineering Research Council of Canada (NSERC Strategic Grant No. 350638), the Fonds québécois de la recherche sur la nature et les technologies (FQRNT), and the Canada Research Chairs (CRC) program. R.F. Domingos acknowledges the support of Fundação para a Ciência e Tecnologia, Portugal, for a Postdoctoral fellowship (SFRH/BPD/37731/2007).

Supporting Information Available: Representative TEM image of TiO_2 particles suspended in 10 mM NaNO_3 electrolyte at pH 3, plots showing calculated DLVO energy profiles for a TiO_2 nanoparticle approaching a flat SiO_2 surface, table with TiO_2 deposition rates onto the silica surface estimated using eq 2, and table with TiO_2 particle diameters used in the calculation of the DLVO interaction energy profiles. This material is available free of charge via the Internet at <http://pubs.acs.org>.

(49) Hahn, M. W.; Abadzic, D.; O'Melia, C. R. *Environ. Sci. Technol.* **2004**, *38* (22), 5915–5924.

(50) Tufenkji, N.; Elimelech, M. *Langmuir* **2004**, *20*, 10818–10828.